J Neurophysiol 93: 2710–2722, 2005.
First published December 29, 2004; doi:10.1152/jn.00636.2004.

Persistent Sodium Currents in Mesencephalic V Neurons Participate in Burst Generation and Control of Membrane Excitability

Nanping Wu,[1] Akifumi Enomoto,[1,2] Susumu Tanaka,[1,3] Chie-Fang Hsiao,[1] Duane Q. Nykamp,[4] Eugene Izhikevich,[5] and Scott H. Chandler[1]

[1]*Department of Physiological Science, University of California, Los Angeles, California;* [2]*1st Department of Oral and Maxillofacial Surgery, Graduate School of Dentistry, Osaka University;* [3]*Department of Oral and Maxillofacial Surgery, Matsumoto Dental University, Nagano, Japan;* [4]*School of Mathematics, University of Minnesota, Minneapolis, Minnesota; and* [5]*The Neurosciences Institute, San Diego, California*

Submitted 23 October 2004; accepted in final form 22 December 2004

Wu, Nanping, Akifumi Enomoto, Susumu Tanaka, Chie-Fang Hsiao, Duane Q. Nykamp, Eugene Izhikevich, and Scott H. Chandler. Persistent sodium currents in mesencephalic V neurons participate in burst generation and control of membrane excitability. *J Neurophysiol* 93: 2710–2722, 2005. First published December 29, 2004; doi:10.1152/jn.00636.2004. The functional and biophysical properties of a persistent sodium current (I_{NaP}) previously proposed to participate in the generation of subthreshold oscillations and burst discharge in mesencephalic trigeminal sensory neurons (Mes V) were investigated in brain stem slices (rats, p7–p12) using whole cell patch-clamp methods. I_{NaP} activated around –76 mV and peaked at −48 mV, with $V_{1/2}$ of –58.7 mV. Ramp voltage-clamp protocols showed that I_{NaP} undergoes time- as well as voltage-dependent inactivation and recovery from inactivation in the range of several seconds (τ_{onset} = 2.04 s, τ_{recov} = 2.21 s). Riluzole ($\leq$5 μM) substantially reduced I_{NaP}, membrane resonance, postinhibitory rebound (PIR), and subthreshold oscillations, and completely blocked bursting, but produced modest effects on the fast transient Na^+ current (I_{NaT}). Before complete cessation, burst cycle duration was increased substantially, while modest and inconsistent changes in burst duration were observed. The properties of the I_{NaT} were obtained and revealed that the amplitude and voltage dependence of the resulting "window current" were not consistent with those of the observed I_{NaP} recorded in the same neurons. This suggests an additional mechanism for the origin of I_{NaP}. A neuronal model was constructed using Hodgkin-Huxley parameters obtained experimentally for Na^+ and K^+ currents that simulated the experimentally observed membrane resonance, subthreshold oscillations, bursting, and PIR. Alterations in the model g_{NaP} parameters indicate that I_{NaP} is critical for control of subthreshold and suprathreshold Mes V neuron membrane excitability and burst generation.

INTRODUCTION

Historically, sodium channels have been identified with rapid, transient action potential production and neuronal electrogenesis. Presently, there are a variety of sodium channel isoforms that can participate, potentially, in more than "all or none" rapid spike production (Waxman 2002). The challenge is to identify a role for each of these unique proteins in neuronal function. It is also clear that, in addition to the fast inward sodium current, there is another type of sodium current that has much slower kinetics and gating properties (Crill 1996). Persistent sodium current (I_{NaP}) is observed in a variety of neuronal types, and in many instances, is slowly inactivating, and is not directly involved in production of the transient action potential. Rather, it is associated with control of membrane excitability in the voltage region just subthreshold to spike production (Boehmer et al. 2000; Chandler et al. 1994; Do and Bean 2003; Taddese and Bean 2002). In tuberomammillary, subthalamic, and suprachiasmatic nucleus neurons, among others, subthreshold sodium current drives spontaneous spike discharge (Do and Bean 2003; Pennartz et al. 1997; Taddese and Bean 2002). Although a role for I_{NaP} was established in some neuron types, the molecular mechanism(s) for production of this current is not clear.

Neuronal bursting is a type of discharge observed in different kinds of neurons during many stereotypic pattern generated behaviors, such as locomotion, respiration, and mastication. Undoubtedly, the bursting mechanism involves the integration of ligand-gated synaptic activity and intrinsic membrane properties. However, in some types of neurons, such as those within the dorsal column nuclei (Reboreda et al. 2003), and trigeminal mesencephalic V nucleus (Wu et al. 2001), burst generation can occur in the absence of synaptic interactions and is associated with subthreshold membrane potential oscillations that are dependent on I_{NaP}.

Recently, using brain stem slices, we showed that mesencephalic trigeminal sensory neurons (Mes V) possess resonant properties (the tendency of the membrane potential to oscillate with a maximal amplitude at a preferred frequency) that underlie the production of subthreshold oscillations and rhythmic burst discharges when depolarized (Wu et al. 2001). We provided evidence that the subthreshold oscillations and burst discharges are generated intrinsically by voltage-gated membrane currents that are not dependent on regenerative calcium conductances. Rather, they result from activation of both transient and persistent subthreshold voltage-dependent sodium currents in combination with steady-state 4-AP sensitive K^+ currents that underlie resonance (Wu et al. 2001). Participation of an I_{NaP} and M-type K^+ currents in production of resonance and theta rhythm has been shown in hippocampal pyramidal cells as well (Hu et al. 2002). Moreover, persistent sodium and K^+ currents contribute, importantly, to subthreshold oscillations in other central neurons (Boehmer et al. 2000; Gutfreund et al. 1995; reviewed in Hutcheon and Yarom 2000; Klink and Alonso 1993). In contrast, calcium currents have been impli-

Address for reprint requests and other correspondence: S. H. Chandler, Dept. of Physiological Science, UCLA, 2859 Slichter Hall, Los Angeles, CA 90095 (E-mail: schandler@physci.ucla.edu).

The costs of publication of this article were defrayed in part by the payment of page charges. The article must therefore be hereby marked "*advertisement*" in accordance with 18 U.S.C. Section 1734 solely to indicate this fact.

 0022-3077/05 $8.00 Copyright © 2005 The American Physiological Society

cated in slow membrane oscillations in some neuron types (Llinas and Yarom 1981; McCormick and Pape 1990).

Activity in trigeminal Mes V neurons can contribute to aspects of oral-motor pattern generation (Kolta et al. 1995). To fully understand how resonance and subthreshold oscillations are integrated to control membrane excitability and bursting in Mes V neurons, it is necessary to characterize in detail the underlying intrinsic currents responsible for their subthreshold and suprathreshold voltage response characteristics and construct neuronal models, using realistic parameters for these currents that simulate the experimental data. Predictions from the model as to the role played by various conductances in control of membrane excitability and spike discharge properties could then be generated and tested experimentally (Butera et al. 1999; Dale 1995). Therefore in this study, we sought to characterize in more detail the biophysical properties of both the fast and slow sodium currents and incorporate these data and previous data obtained on potassium currents (Del Negro and Chandler 1997) into a neuronal model that simulates the experimental observations. Using pharmacological, electrophysiological, and neuronal modeling techniques, we show that I_{NaP} *1*) is critical for amplification of membrane resonance, *2*) necessary for burst generation, *3*) is not solely generated by a fast transient sodium "window current," and *4*) in conjunction with a resonant voltage-dependent K^+ current can be incorporated into a realistic computer neuronal model to simulate the salient features of membrane resonance, subthreshold oscillations, postinhibitory rebound (PIR), and bursting behavior.

METHODS

Coronal slices from neonatal Sprague-Dawley rats were cut as described previously (Wu et al. 2001). Briefly, animals were rapidly decapitated. The brains were quickly removed and immersed in oxygenated (95% O_2-5% CO_2) ice-cold cutting solution of the following composition (in mM): 126 NaCl, 3 KCl, 1.25 NaH_2PO_4, 26 $NaHCO_3$, 10 glucose, 1 $CaCl_2$, 5 $MgCl_2$, and 4 lactic acid (Schurr et al. 1988). The pH of the external solutions was between 7.3 and 7.35. The brain stem was glued by its rostral end to the platform of a chamber and covered with ice-cold cutting solution. Six slices (300 μm) were cut on a vibrating slicer (DSK microslicer, Ted Pella, Redding, CA), placed into an oxygenated incubation solution (37°C) of the following composition (in mM): 124 NaCl, 3 KCl, 1.25 NaH_2PO_4, 26 $NaHCO_3$, 10 glucose, 2 $CaCl_2$, 2 $MgCl_2$, and 4 lactic acid (Schurr et al. 1988) for 40–50 min and maintained at room temperature (22–24°C) until used.

Electrophysiological technique

Patch electrodes were fabricated from borosilicate glass capillary tubing (1.5 mm OD, 0.86 mm ID) using a Model P-97 puller (Sutter Instrument, Navato, CA). Tip resistances were 2–4 MΩ when filled with a solution containing (in mM) 115 K-gluconate, 25 KCl, 9 NaCl, 10 HEPES (base), 0.2 EGTA, 1 $MgCl_2$, 3 K_2-ATP, and 1 Na-GTP, pH ≈ 7.25, osmolarity adjusted to 280–290 mOsm. To isolate I_{NaP} during voltage-clamp experiments, K^+ currents were blocked using an intrapipette solution containing (in mM) 130 CsF, 9 NaCl, 10 HEPES (base), 10 EGTA, 1 $MgCl_2$, 3 K_2-ATP, and 1 Na-GTP. The control external solution consisted of ACSF of the following composition (in mM): 124 NaCl, 3 KCl, 1.25 NaH_2PO_4, 26 $NaHCO_3$, 10 glucose, 2 $CaCl_2$, and 2 $MgCl_2$. External solutions for I_{NaP} isolation contained (in mM) 131 NaCl, 10 HEPES (base), 3 KCl, 10 glucose, 1 $CaCl_2$, 2 $MgCl_2$, 10 tetraethylammonium (TEA)-Cl, 10 CsCl, 1–3 4-aminopyridine (4-AP), and 0.3 $CdCl_2$. External solutions for I_{NaT} isolation contained (in mM) 15 NaCl, 10 HEPES (base), 2 $BaCl_2$, 1 $MgCl_2$, 110 TEA-Cl, and 0.3 $CdCl_2$. In selected experiments, TTX (0.01–0.5 μM) or riluzole (0.5–200 μM) was applied to the bath. All drugs were purchased from Sigma (St. Louis, MO).

Whole cell current and voltage-clamp recordings were performed with an Axopatch-1D amplifier (Axon Instruments, Foster City, CA) in concert with pCLAMP acquisition software (v8.0, Axon Instruments). Cells with seals <1 GΩ before breakthrough were discarded. Uncompensated series resistance was usually <10 MΩ, compensated 60–80%, and monitored periodically throughout the experiment. Data were low-pass filtered at 2 (V-clamp) or 5 KHz (I-clamp) (−3 dB 4-pole Bessel filter) and sampled at 1–10 KHz depending on the experiments. The liquid junction potentials (measured with a 3 M KCl reference electrode) for K^+ gluconate– and CsF-based electrodes were −6 and −7 mV, respectively, and corrected off-line (Zhang and Krnjevic 1993).

Slices were perfused with oxygenated artificial cerebrospinal fluid (ACSF; 2 ml/min) at room temperature and visualized by infrared differential interference contrast microscopy (Stuart et al. 1993). The Mes V nucleus was identified bilaterally in the coronal slice under low magnification (×5) as an ellipsoid region, located dorsally in brain stem slices ~500 μm lateral to the midline. Mes V neurons were easily distinguished based on their location, pseudounipolar soma, and size (Del Negro and Chandler 1997; Henderson et al. 1982). The effects of drugs applied to the bath solution were obtained after 3 ~ 10 min from onset of application. Recording periods were usually between 30 and 90 min.

Frequency-domain analysis (Puil et al. 1986, 1988) was performed by injecting a computer generated input current of constant amplitude but linearly varying frequencies (ZAP current) between 0 and 250 Hz into neurons and recording the resulting voltage responses as described in detail previously (Wu et al. 2001). Currents were adjusted to produce voltage responses below spike threshold. From this, impedance was calculated as the ratio of the fast Fourier transform (FFT) of the voltage response and the input current using the following formula: $Z = \mathrm{FFT}(V)/\mathrm{FFT}(I)$. The magnitude of the impedance was plotted against frequency to give a frequency-response curve (FRC). The ZAP input current was generated with the following formula: $I(t) = a \times \sin(bt^3)$, $0 < t < T$. Here, a and b are adjustable parameters controlling the amplitude and bandwidth of the input current, respectively. A low-pass filter was used to reduce the noise of the current. The results with and without the filter were identical.

Data were collected and analyzed with a combination of software [Clampfit (v8.0, Axon Instruments), Datapac III (v1.1, Run Technologies, Irvine, CA), StatView (SAS Institute, Cary, NC), and Microsoft Excel]. Results are reported as mean ± SD, unless indicated otherwise. Unless specified, group comparison of mean values were performed with Student's t-test set at a level of significance of $P < 0.05$.

Model

We use a single compartment Hodgkin-Huxley-type model consisting of the following currents

$$C\frac{dV}{dt} = I - I_{Leak} - I_K - I_{NaT} - I_{NaP} + \mathrm{noise}(t)$$

where

$$I_{Leak} = g_{Leak}(V - E_{Leak})$$

$$I_K = \bar{g}_K n(V - E_K)$$

$$I_{NaT} = \bar{g}_{NaT} m_{t,\infty}(V) h_t (V - E_{Na})$$

$$I_{NaP} = \bar{g}_{NaP} m_{p,\infty}(V) h_p (V - E_{Na})$$

and

$$\frac{dn}{dt} = [n_\infty(V) - n]/\tau_K(V) \text{ (fast)}$$

$$\frac{dh_t}{dt} = [h_{t,\infty}(V) - h_t]/\tau_{NaT}(V) \text{ (fast)}$$

$$\frac{dh_p}{dt} = [h_{p,\infty}(V) - h_p]/\tau_{NaP}(V) \text{ (slow)}$$

Thus I_{NaT} and I_{NaP} have instantaneous activation kinetics and relatively slower inactivation kinetics. We also explored the case of noninstantaneous activation kinetics having time constants <1 ms and found that they do not affect the results.

Experimentally measured parameters for (in)activation curves, time constants, and maximal conductances resulted in

$$n_\infty(V) = \frac{1}{1 + e^{-(V+43)/3.9}}$$

$$\tau_K(V) = 4$$

$$m_{t,\infty}(V) = \frac{1}{1 + e^{-(V+31.3)/4.3}}$$

$$h_{t,\infty}(V) = \frac{1}{1 + e^{(V+55)/7.1}}$$

$$\tau_{NaT}(V) = 3$$

$$m_{p,\infty}(V) = \frac{1}{1 + e^{-(V+50)/6.4}}$$

$$h_{p,\infty}(V) = \frac{1}{1 + e^{(V+52)/14}}$$

$$\tau_{NaP}(V) = 1{,}000 + \frac{10{,}000}{1 + e^{(V+60)/10}}$$

and $E_{Leak} = 60$ mV, $E_{Na} = 55$ mV, $E_K = 92$ mV, $g_{Leak} = 2$, $\bar{g}_{NaT} = 12$, $\bar{g}_{NaP} = 1.1$, $\bar{g}_K = 6$, and $C = 1$. To simulate membrane noise, we inject the current noise (t) governed by the Ornstein-Uhlenbeck process noise(t)' = −noise(t) + 3$\xi(t)$, where $\xi(t)$ is a random variable with normal distribution, zero mean, and unitary variance. All simulations were performed using MATLAB and XPPAUT.

RESULTS

Electrophysiological recordings were performed on 243 Mes V neurons from brain slices of rat. The zero current holding potential was –63 ± 3.0 mV, the input resistance was 144.8 ± 108.1 MΩ, and membrane capacitance was 53.9 ± 15.0 pF (n = 157).

I_{NaP} in Mes V neurons

Initially, to isolate I_{NaP}, we applied depolarizing voltage ramps from –90 to 10 mV within 3 s (33.3 mV/s) in voltage-clamp mode (Fig. 1*A*). The rising rate of voltage ramps was slow enough to inactivate I_{NaT}. The resultant *I-V* relationship was inward from approximately –70 mV and abolished by 0.5 μM TTX application, indicating the presence of I_{NaP} over that time period. At potentials more positive than –45 mV, I_{NaP} was superimposed on an outward current previously described as a nonspecific cation current I_{cat} (Alzheimer 1994; Fleidervish and Gutnick 1996). In the presence of TEA and Cd^{2+}, I_{cat} was the only voltage-dependent current that remained when TTX was added to the bath (Fig. 1*A*). Activation of this current occurred at approximately –47 ± 7.3 mV, (n = 42). Digital subtraction of the trace before and after TTX application yielded the *I-V* curve representing I_{NaP} (Fig. 1*A*, difference

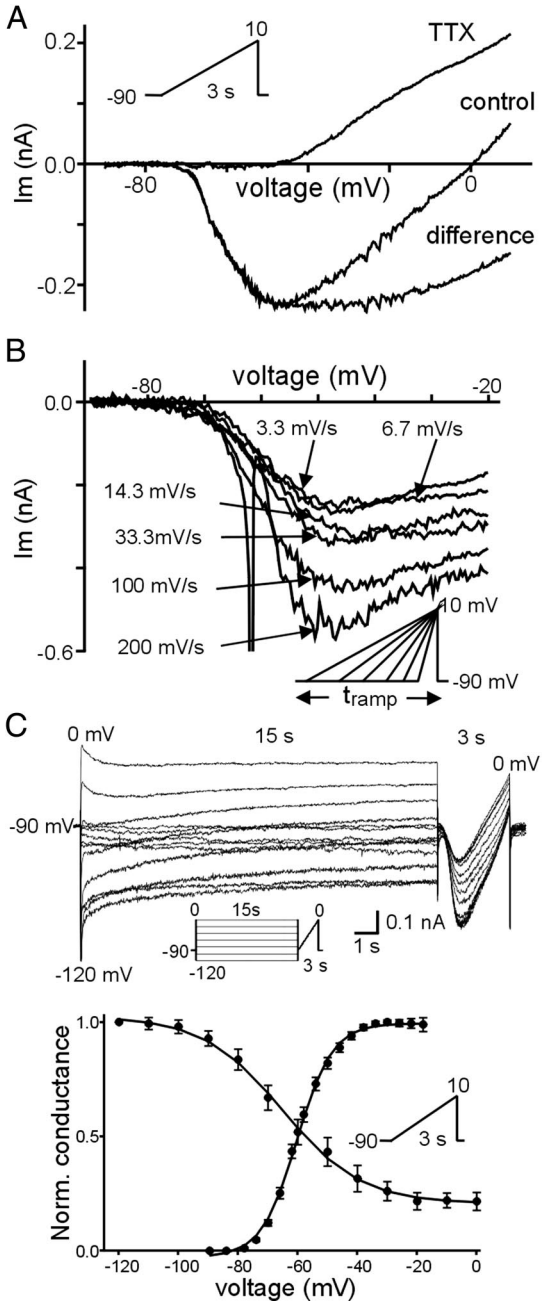

FIG. 1. Properties of I_{NaP} in mesencephalic trigeminal sensory neurons. *A*: slow ramp from –90 to 10 mV (33.3 mV/s) evoked inward current that was TTX (0.5 μM) sensitive (TTX-subtracted I_{NaP} is labeled "difference"). *B*: TTX-subtracted I_{NaP} peak amplitude decreased as a function of ramp rate. *Inset*: ramp protocol. Note that here, as well as for all of the voltage-clamp protocols, the neuron was clamped at –90 mV for 30 s before the onset of the next test ramp to allow recovery from the inactivation that developed during the foregoing cycle. *C*: voltage dependence of activation and inactivation of I_{NaP}. Single Boltzmann function is fit to mean normalized conductance (activation, n = 39), with $V_{1/2}$ = –57.9 mV and k = –6.4 mV and for inactivation, $V_{1/2}$ = –58.7 mV and k = 14.2 mV (n = 11). For inactivation protocol, the conditioning pulse (15 s) preceding each ramp varied from –120 to 0 mV in 10-mV steps. Activation and inactivation protocols are shown in *inset*.

trace). In Mes V neurons, I_{NaP} activated around –76 ± 4 mV and peaked at –48 ± 8 mV (n = 49). I_{NaP} peak amplitude varied widely from cell to cell (range, –133.7 to –918.7 pA; median, −337.5 pA; n = 49). However, when the currents were normalized for differences in cell size, as indicated by changes in cell capacitance, we found that current density was between 4.6 and 6.9 pA/pF.

The use of ramp, as opposed to step, protocols allowed us to rapidly generate a contiguous *I-V* relationship for slowly changing currents in a short time period. However, depending on the ramp speeds, the currents generated by this protocol could be contaminated by I_{NaT} due to inadequate voltage clamp. Therefore in a subset of experiments, we measured the amplitude of the membrane current at −45 mV (approximate voltage where peak I_{NaP} occurs) obtained with a ramp protocol. In the same neuron, we compared that current to the current obtained by the use of a traditional step protocol measured at 200 ms following the onset of the step pulse and after the transient spike completely inactivated. We found that the mean currents were comparable (step −98.5 ± 24.2 pA vs. ramp −94.8 ± 25.4 pA, n = 3), suggesting that at these slow ramp speeds (33 mV/s), the adequacy of the clamp was very good, and the currents were not contaminated by activation of I_{NaT}.

In the initial experiments we noticed that the peak amplitudes of I_{NaP} got larger with faster ramps, indicating some degree of slow inactivation of I_{NaP} occurred during slower ramps. Therefore it was necessary to examine in more detail the properties of I_{NaP} inactivation since this property could contribute in conjunction with other ionic currents to burst termination and control of burst cycle duration during rhythmic burst activity. The time-dependent changes in I_{NaP} were examined by applying a series of voltage ramps with different rates of rise. As shown in Fig. 1*B*, although repetitive spiking and associated escapes from voltage clamp appeared in the current trace during a very brief ramp from –90 to 10 mV (Fig. 1*B*; 200 mV/s), fast inactivation of I_{NaT} was complete at ramp rates slower than 100 mV/s, similar to that shown elsewhere (Fleidervish and Gutnick 1996). When ramps of 100 mV/s and slower were applied, I_{NaP} decreased as a function of ramp rate, suggesting time-dependent slow inactivation of I_{NaP}. A quasi-steady-state condition was achieved at rates between 3.3 and 6.7 mV/s, indicating a component of I_{NaP} that did not inactivate, and was truly persistent. To study the properties of the inactivating component of I_{NaP}, in subsequent experiments, ramps of 33.3 mV/s were used as an optimal stimulus. At this speed, the ramp was slow enough to permit adequate voltage control and induce complete inactivation of I_{NaT}, yet fast enough to prevent complete inactivation of the slowly inactivating component during the course of the ramp.

The voltage dependence of I_{NaP} activation, based on ramp stimuli, is plotted as a function of command potential (E_C) in Fig. 1*C* for 39 neurons. The normalized conductance (G) was determined by the equation

$$G = I/(E_c - E_{rev})$$

where I represents the subtracted I_{Na}, and E_{rev} is the reversal potential for Na^+ (64.8 mV) calculated from the solution composition at 22°C. Conductance was normalized to the maximal conductance for each neuron. Data points were fit with a Boltzmann function that yielded a mean half-activation potential ($V_{1/2}$) of –57.9 ± 3.0 mV (n = 39) and a slope factor k of –6.4 ± 2.1 mV.

The voltage dependence of slow inactivation is summarized in Fig. 1*C* (protocol shown in *inset*), using prepulses of 15-s duration. The peak amplitude of the current reached a plateau value around –100 mV and gradually decreased with more depolarized conditioning pulses. The mean TTX-sensitive normalized peak conductance was plotted against conditioning pulse potential and fit with a Boltzmann equation. From such data, $V_{1/2}$ = –58.7 ± 8.7 mV (n = 9) and k = 14.2 ± 3.6 mV. Note that the inactivation was not complete even at conditioning potentials held at 0 mV.

Time dependence of I_{NaP} inactivation and recovery from inactivation

The time dependence of onset of slow inactivation was first analyzed by means of a prepulse ramp protocol (Fig. 2*A*, *top*). An example of the superimposed traces of current responses before and during a ramp delivered without a conditioning pulse and after a 10-s step to 20 mV are shown in Fig. 2*A* (*bottom*). A test ramp applied 50 ms after the termination of the conditioning pulse (to remove fast inactivation) revealed that the I_{NaP} was depressed at most potentials compared with control. The superimposed traces in Fig. 2*B* show the effect on the peak amplitude of I_{NaP} by systematically varying the duration of the conditioning pulse. To avoid trial-to-trial accumulation of slow inactivation, the protocol was repeated every 30 s. The resultant plots of I_{NaP} (normalized to control peak current) as a function of prepulse duration give the time course of onset of slow inactivation of I_{NaP}, which was fit to a single exponential (Fig. 2*C*, τ = 2.04 s; n = 11). Note that slow inactivation of I_{NaP} was never >75%, even after the most prolonged prepulse of 10 s. A similar result was observed in

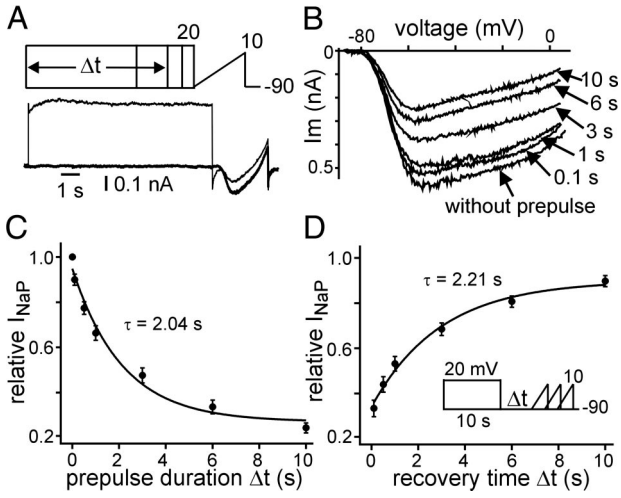

FIG. 2. Time course of onset and recovery of I_{NaP} inactivation. *A* and *B*: I_{NaP} amplitude declined as a function of the prepulse duration. Voltage protocol (*A, top*) and superimposed current traces before and during 33.3 mV/s depolarizing voltage ramp from –90 to 10 mV without and after 10-s conditioning pulse to +20 mV (*A, bottom*). *B*: raw current data for different conditioning prepulse durations. *C*: plots of I_{NaP} as a function of prepulse duration. Data points are normalized mean I_{NaP} peak current values (n = 11 neurons). Solid curve is single exponential best fit to the data with τ = 2.04 s. *D*: time course of recovery from slow inactivation after a 10-s depolarizing prepulse to +20 mV followed a single exponential time course with τ = 2.21 s (n = 11).

mouse neocortical layer V neurons (Fleidervish and Gutnick 1996).

Figure 2*D* summarizes the experiments to determine the time course of recovery of I_{NaP} from slow inactivation (protocol shown in *inset*). Normalized mean peak current amplitudes were used for constructing plots of time dependence of recovery from inactivation (Fig. 2*D*). Those plots show that recovery from slow inactivation followed a single exponential time course with $\tau = 2.21$ s ($n = 11$).

Window current contribution to I_{NaP}

To test the hypothesis that I_{NaP} results from a "window current," a component arising from the overlap of the steady-state activation and inactivation variables of g_{NaT}, we calculated the theoretical window current contribution from the product of the activation and inactivation variables obtained from the Boltzmann fits of the I_{NaT} in low external Na^+ conditions (15 mM) and compared that to the measured I_{NaP} in the same neurons. In these experiments it is important that the fast transient spike is adequately clamped to obtain accurate measurements of I_{NaT} window current for comparison with I_{NaP}. During these conditions, the maximal I_{NaT} was ~1.6 nA. Considering that the maximal uncompensated series resistance never exceeded 10 MΩ (typically <5 MΩ) and is routinely compensated to 80% in this subset of experiments, the maximal voltage error of the fast spike would be ~3.2 mV. To estimate the time constant of voltage settling after initiation of a step pulse, the compensated series resistance was multiplied by the mean capacitance of these neurons (54 pF). This produced a time constant of ~100 μs and 98% of the target voltage would be obtained within 400 μs (4 × tau). Errors due to faulty space clamp are minimized since Mes V neurons are essentially spheres, with few, if any dendrites and a stem axon that is cut in the slice. Despite these precautions, one should still be cautious in interpreting voltage clamp data under these conditions.

Figure 3*A* shows sodium current traces recorded from a representative neuron in response to activation and inactivation pulse protocols (*inset*). Peak current amplitudes were measured and used for deriving conductance values. Figure 3*B* shows an example of a steady-state activation (●) and inactivation (○) plot for the TTX-sensitive I_{NaT} and fitted with Boltzmann functions (solid lines). Compared with I_{NaP}, $V_{1/2}$ was more positive (–43.4 ± 0.3 mV), but the slope factor ($k = –5.0 \pm 0.2$ mV, $n = 24$) was about the same. Interestingly, the $V_{1/2}$ for inactivation of I_{NaT} (–61.5 ± 0.2 mV) was approximately equal to that of I_{NaP}, but the slope of the inactivation plot was much steeper for I_{NaT} ($k = 8.1 \pm 0.2$ mV, $n = 25$).

As shown in Fig. 3*B*, a typical steady-state activation and inactivation curve for I_{NaT} exhibited a region of overlap between a narrow voltage range from –65 to –35 mV, forming a window current. Superimposed is the theoretical window current normalized to the maximum value obtained from the product of the Boltzmann functions for activation and inactivation (dotted line). To estimate the contribution of this current to the measured persistent currents, we compared this window current with I_{NaP} recorded from the same cell. To minimize voltage clamp errors, both I_{NaT} and I_{NaP} were recorded in external solution with 15 mM Na^+. In Mes V neurons, the mean amplitude of the theoretically predicted peak window

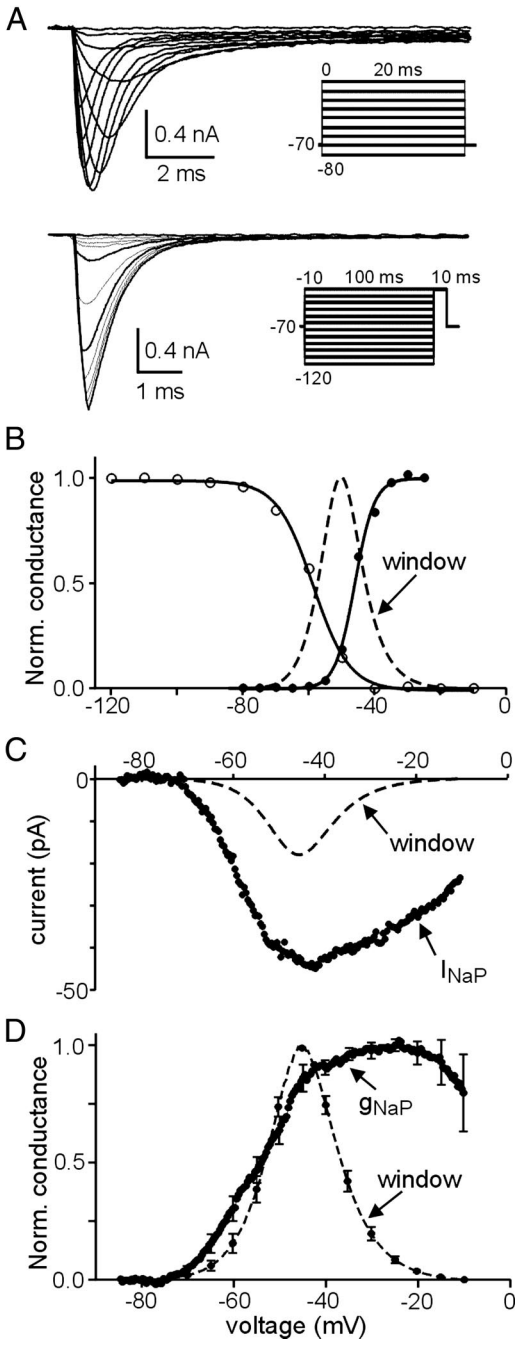

FIG. 3. I_{NaP} is not determined by a classical Hodgkin-Huxley window current. *A*: fast sodium current (I_{NaT}) traces evoked during activation (*top*) and inactivation (*bottom*) protocols from a holding potential of –70 mV obtained in low external Na^+ solution (15 mM). Duration of the conditioning prepulse was 100 ms during the inactivation protocol. *B*: plots of the voltage dependence of inactivation (○) and steady-state activation (●) of I_{NaT} for the same cell in *A*. G_{NaT} plots were normalized for the maximal values and each fitted with a single Boltzmann function (continuous lines). Fitting parameters were $V_{1/2} = –60.1$ mV, $k = 7.1$ mV (steady-state inactivation); $V_{1/2} = –43.4$ mV, $k = –5.0$ mV (activation). Predicted normalized window conductance is also shown (dotted line, product of activation and inactivation curves). *C*: amplitude of I_{NaP} evoked by a slow voltage ramp (33.3 mV/s; TTX-subtracted) is compared with that of theoretically predicated window current in the same cell as in *A* and *B*. *D*: summary voltage dependence of the experimentally obtained conductance (g_{NaP}) is plotted with that of the calculated window conductance (dotted line) for 5 neurons. Both conductances have been normalized to the maximal values.

current was –22.3 ± 10.4 pA [2.6% of the maximum peak transient current ($I_{NaT\text{-}Max}$, –1591 ± 292 pA)], and occurred at –50.4 ± 0.9 mV ($n = 5$). The peak I_{NaP} (–61.8 ± 21.7 pA) occurred at –43.8 ± 5.9 mV, and was ~3.9% of the peak $I_{NaT\text{-}Max}$. At the maximum of I_{NaP} (near –44 mV), the mean contribution of the window current was ~37% of the total I_{NaP} (4.7–55.5%, $n = 5$). Figure 3*C* shows a representative example of a comparison between the measured I_{NaP} and the theoretically calculated window current in the same cell, suggesting that the window current does contribute to, but cannot account for all, of the I_{NaP} in this cell. Moreover, at the more depolarized membrane potentials where the window current was <1 pA (near –27 mV, $n = 5$), the level of I_{NaP} was ~79% of its peak current. This difference is shown more clearly when a composite summary of the normalized underlying conductances are plotted as a function of voltage for five neurons (Fig. 3*D*). At voltages where the mean window current conductances declined, the I_{NaP} conductance was still very large. The difference in voltage dependence and amplitude of these currents suggests that, although the window current makes some contribution to I_{NaP} in Mes V neurons, I_{NaP} is not solely determined by the window current. Similar conclusions were made for other neurons (Alzheimer et al. 1993; Baker and Bostock 1997; Maurice et al. 2001).

Riluzole suppresses I_{NaP}

Although I_{NaP} is observed in various types of neurons, the precise channel mechanisms responsible for this current are still not clear (see Goldin 2001), and there is no specific drug that unambiguously separates I_{NaP} from I_{NaT}. However, in rat cortex at concentrations <10 μM, riluzole (2-amino-6-trifluoromethoxy benzothiazole, RP54274), suppresses I_{NaP} to a greater extent than I_{NaT} (Urbani and Belluzzi 2000). If this applies for Mes V neurons as well, this would be a useful compound to investigate the physiological role for I_{NaP} in control of Mes V membrane excitability. Therefore to test this possibility, the following experiments were performed.

Figure 4, *A1* and *B1,* shows the typical effects of riluzole on I_{NaT} and I_{NaP}, whereas the summary dose-response relationship for riluzole on the peak I_{NaT} is shown in Fig. 4*A2*. The EC_{50} for suppression of I_{NaT} was 51.6 μM, and 200 μM produced maximal suppression. At concentrations of 2 and 5 μM, riluzole reduced the peak I_{NaT} by 5.2 ± 1.2 and 11.3 ± 0.5% ($n = 5$), respectively (Fig. 4*A2*). Additionally, riluzole had no effect on $h\infty$ (Fig. 4*A3*, dotted line), indicating that fast sodium channel steady state availability was not compromised. In contrast, riluzole suppressed I_{NaP} by 53% of its peak at 2 μM ($n = 9$) and 81% at 5 μM ($n = 11$; Fig. 4*B2*). Accordingly, we

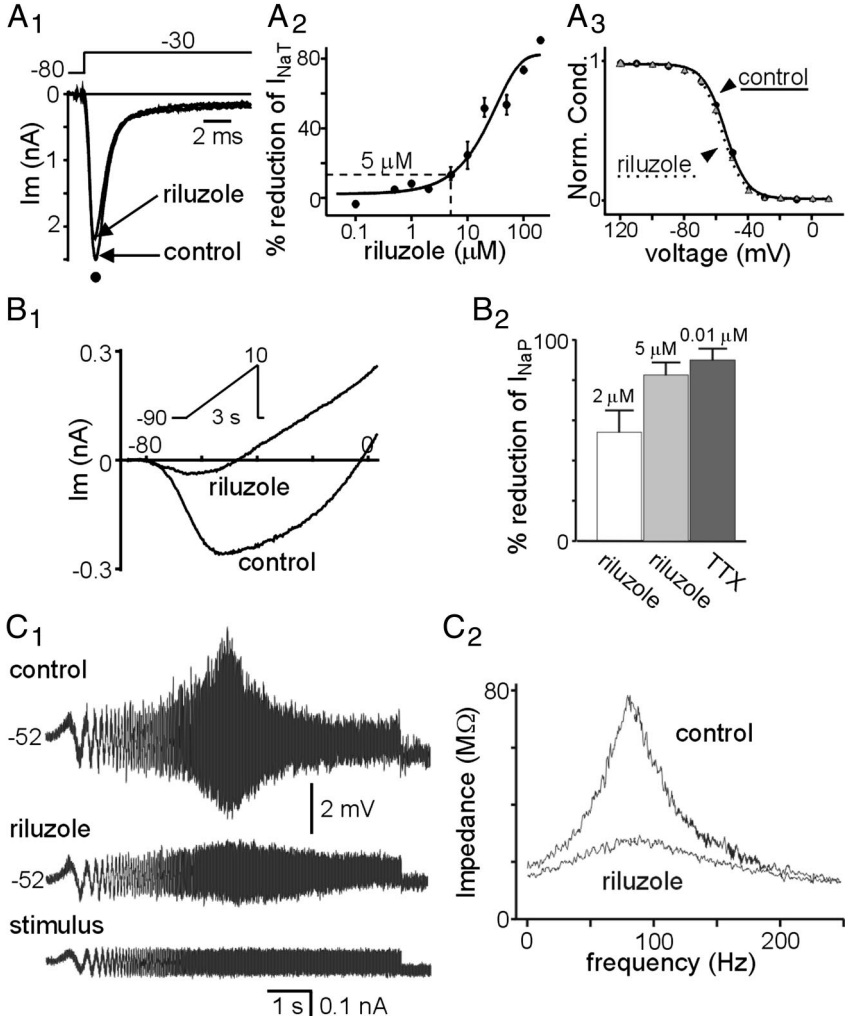

FIG. 4. Riluzole suppresses I_{NaP} in Mes V neurons. *A1*: TTX-sensitive fast Na^+ current was reduced, minimally, after riluzole application (recorded in modified low Na^+ external solution; 60 mM). *A2*: dose-response relationship for riluzole effects on peak I_{NaT} ($n = 5$). EC_{50} = 51.6 μM. *A3*: availability curve for the I_{NaT} before (solid line), and during riluzole (dotted line) application. *B1*: effects of riluzole on I_{NaP} *I-V* relationship. *B2*: histogram of percent reduction by riluzole or TTX on I_{NaP}. *C1*: a typical example of effects of riluzole on subthreshold membrane potential in response to ZAP input current stimulus (see METHODS) before and after riluzole. Frequency of stimulus varied from 0 to 250 Hz. *C2*: frequency-response curve (FRC) derived from data shown in *C1*. Application of 5 μM riluzole reduced the impedance magnitude substantially at depolarized potential but did not abolished the hump or peak frequency of FRC.

used ≤5 μM riluzole to suppress I_{NaP} in the additional experiments described below.

Functional consequences of I_{NaP} suppression on membrane excitability

Previously, we proposed that high-frequency membrane resonance is the basis for subthreshold oscillations and high-frequency spike discharge, as well as conditional rhythmic burst generation in Mes V neurons (Wu et al. 2001). Additionally, we proposed that the emergence of subthreshold oscillations results from activation of a slowly or noninactivating Na^+ current that produces amplified resonance (Hutcheon and Yarom 2000). Since riluzole at 5 μM blocks I_{NaP} predominately, as opposed to I_{NaT}, we sought to obtain more direct evidence that I_{NaP} is critical for control of subthreshold membrane excitability and maintenance of high-frequency spike discharge and bursting.

The importance of I_{NaP} in amplifying membrane resonance is shown in Fig. 4, *C1* and *C2*. A ZAP current function (Puil 1986; Wu et al. 2001) was applied, and the subsequent effects on low-amplitude sinusoidal voltage changes before burst onset were examined. The amplitude of the current was adjusted to produce voltage changes <5 mV from the holding potential. An example of the raw data are shown in Fig. 4*C1,* where the membrane potential was artificially held at –52 mV, a level subthreshold for burst generation. The subsequent impedance-frequency curve (FRC) is plotted in Fig. 4*C2*. The control record shows a resonant peak at ~75 Hz in this example, typical of Mes V neurons (Wu et al. 2001). Riluzole (5 μM) suppressed, but did not abolish, the resonant peak amplitude, and did not alter significantly the low frequency impedance, indicating that I_{NaP} is capable of amplifying membrane resonance but is not the resonant current. To determine if subthreshold oscillations and conditional rhythmic bursting emerge from amplified membrane resonance due to I_{NaP}, as proposed previously (Wu et al. 2001), the effects of riluzole were examined on those membrane behaviors.

Figure 5*A* shows the typical observation that riluzole blocked conditional membrane bursting in response to maintained membrane depolarization within 2–4 min of application ($n = 12$). To examination this observation in more detail, in a subset of five neurons, we applied a current pulse that was just suprathreshold to induce precisely five consecutive bursts (~16 s). We repeated this control protocol four times over a period of 5–6 min to insure that stable, rhythmical bursting was consistently induced and not deteriorating over that time period (Fig. 5*C*). For each trial, we calculated the mean burst duration (BD) and cycle duration (CD) for the last four consecutive bursts. Once it was determined that the responses were stable over four trials, 0.5 μM riluzole was applied, and the same protocol was repeated. Before complete cessation of bursting, which usually occurred within 3–5 min, the main effect on cycle characteristics was a significant prolongation of CD (~60% above controls, $P < 0.01$, Fisher post hoc) and a modest, but not significant, decrease in BD (~10%, $P > 0.1$). Interestingly, this is similar to the effects predicted by the model simulations when g_{NaP} was reduced sufficiently to abolish bursting (Fig. 10). The normalized cycle and burst duration data are summarized in Fig. 5*C* for five neurons.

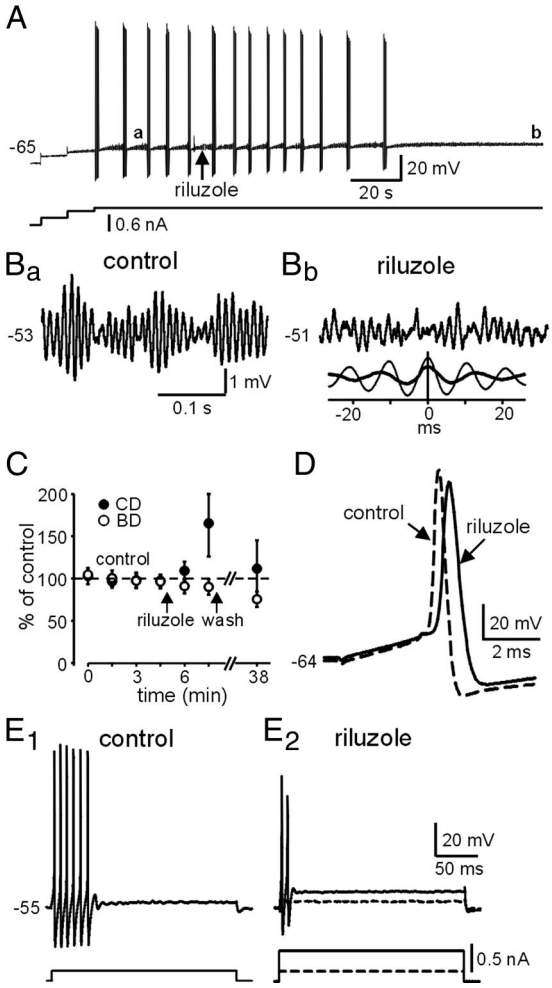

FIG. 5. Riluzole suppresses the amplitude of subthreshold oscillations and abolishes conditional rhythmic burst discharge. *A*: maintained rhythmic burst discharge in response to membrane depolarization was abolished by riluzole application (arrow). *Bottom trace* is current stimulus. *B*: high gain records of segments of membrane potential taken from *A,* labeled with lowercase letters. Riluzole application dramatically suppressed the amplitude of the subthreshold oscillations without effect on peak frequency (*inset*: auto-correlation, thick line represents riluzole condition). *C*: graph of normalized cycle duration (CD) and burst duration (BD) before, during, and after riluzole application. Washout was measured after 30 min. Horizontal dotted line at 100% represents mean of control values ($n = 5$ neurons). *D*: superimposed traces before and after riluzole application evoked by a short current pulse (3 ms). *E*: voltage changes in response to a depolarizing step pulse (250 ms, 0.2 nA) recorded before (*E1*) and after (*E2*) riluzole application. Current stimuli are shown at *bottom*.

Figure 5*B* shows the effects of riluzole on subthreshold oscillations before (Fig. 5*Ba*, taken at *Aa*), and during drug application (Fig. 5*Bb*, taken at *Ab*). Clearly, the amplitude of the oscillations, as indicated by the autocorrelation (Fig. 5*Bb*), was reduced substantially (control: 4.7 ± 0.6 mV; riluzole: 1.9 ± 0.6 mV, $n = 5$, $P < 0.01$), without significant effects on the frequency of the oscillations (control: 93 ± 7 Hz; riluzole: 90 ± 18 Hz, $n = 5$, $P = 0.70$). It is unlikely that the effects on bursting resulted from complete suppression of the action potential since during these conditions in response to a 3-ms current pulse the evoked action potential threshold and amplitude were modestly affected ($n = 12$; Fig. 5*D*; Table 1). This is consistent with the minimal effects of riluzole on activation and inactivation of I_{NaT} shown in Fig. 4*A*.

TABLE 1. *Effects of riluzole on action potential*

	n	RMP, mV	Threshold, mV	Peak, mV	Half-width, ms
Control	12	−59 ± 4	−46 ± 3	106 ± 11	0.55 ± 0.09
Riluzole	12	−57 ± 6	−42 ± 7	93 ± 12*	0.65 ± 0.09*

Values are means ± SD. *Paired *t*-test, $P < 0.01$.

Previously, we showed that the resonant membrane frequency determines the frequency of the subthreshold oscillations, which are significantly correlated with the intraburst spike frequency (Wu et al. 2001). The significant reduction in amplitude, as opposed to frequency, of the subthreshold oscillations after riluzole predicts that mean spike frequency within a burst should be affected minimally after riluzole application. This was confirmed in three neurons where the percent change in mean intraspike frequency within the last burst before complete cessation compared with control was −9.1, 2.0, and −3.0%. Additionally, the percent change in ratio of the last interspike interval to the first interspike interval within a burst was also minimally affected after drug application for the three neurons examined (12.3, 0.3, −8.1%).

The effects of riluzole on stimulus-evoked spike trains are shown in Fig. 5, *E1* and *E2*. As shown, at a holding potential of –55 mV, a 250-ms pulse produced a brief, rapidly adapting spike train (Fig. 5*E1*), as described previously (Del Negro and Chandler 1997). In the presence of riluzole, in only one of eight neurons examined was it possible to evoke a spike train of two or more spikes with further increases in current intensity, as shown in Fig. 5*E2*. However, it was possible to evoke a single action potential in all neurons tested.

Previously, we proposed that slow inactivation of I_{NaP} might contribute to burst termination in addition to other currents (Wu et al. 2001). To obtain evidence for this hypothesis, we examined I_{NaP} induced by slow ramps before, and immediately following, a conditioning voltage waveform resembling a burst discharge obtained during current clamp. This allowed us to more accurately simulate physiological conditions. To achieve this, in each neuron, we first recorded a representative spike burst in current clamp and replayed that as the command voltage waveform immediately before running the ramp protocol to induce I_{NaP}. We then compared the peak amplitude of I_{NaP} before, and immediately following, the conditioning burst waveform. Similar methods using the action potential clamp have been used by others (Do and Bean 2003). Figure 6 shows a representative example. The *top traces* show the waveform protocol, and the *bottom traces* show the recorded persistent current. Based on five neurons examined, the peak amplitude of the ramp current was reduced to ~86 ±10.0% of control immediately following the burst ($P < 0.03$, $n = 5$), suggesting that a reduction in I_{NaP} during a maintained burst could contribute, modestly, to burst termination. The model data support this conclusion.

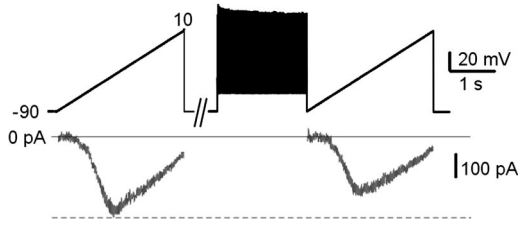

FIG. 6. Slow inactivation of I_{NaP} current following simulated burst discharge. Action potential burst discharge recorded in current clamp was used in voltage clamp as the command waveform. Slow ramp elicited I_{NaP} before, and immediately following, action potential burst clamp. Notice the reduction in I_{NaP} following the burst. I_{NaP} was obtained by subtraction of TTX-sensitive current.

As predicted from the relatively depolarized $V_{1/2max}$ of the $h\infty$ curve for I_{NaP} (Fig. 1), Mes V neurons exhibited postinhibitory rebound (PIR) at membrane potentials close to burst threshold (–52 ± 3 mV; range, –59 to –47 mV, $n = 21$). This response was exquisitely sensitive to small amplitude, short-duration hyperpolarizing pulses (2–1,000 ms) that altered the membrane potential by as little as 3 mV (3.2 ± 1.7 mV, $n = 23$). In this example, application of a small amplitude, short-duration (250 ms) hyperpolarizing pulse produced a robust PIR (Fig. 7*A*). The response was completely blocked by riluzole (Fig. 7*A*), suggesting a role for I_{NaP} in initiation of PIR. In the presence of the I_h blocker ZD 7288 (10 μM), the mean duration of the burst for five neurons was reduced 20 ± 62%, but never blocked (Fig. 7*B*). This reduction most likely resulted from nonspecific effects of ZD, as opposed to block of I_h, since voltage sag, indicative of I_h, was not observed before drug application, and I_h activates at voltages more negative than −70 mV in these neurons (Tanaka et al. 2003). In the presence of cadmium to block calcium currents including T type (I_T), PIR was still observed (Fig. 7*C*), showing that this response is not initiated by low-threshold transient calcium conductances such as I_T. In fact, in the presence of Cd^{2+}, the PIR response was enhanced in duration by 299 ± 186% ($n = 4$) and most likely resulted from a decrease in a calcium-activated K^+ conductance, as previously described in these neurons (Del Negro and Chandler 1997; Wu et al. 2001).

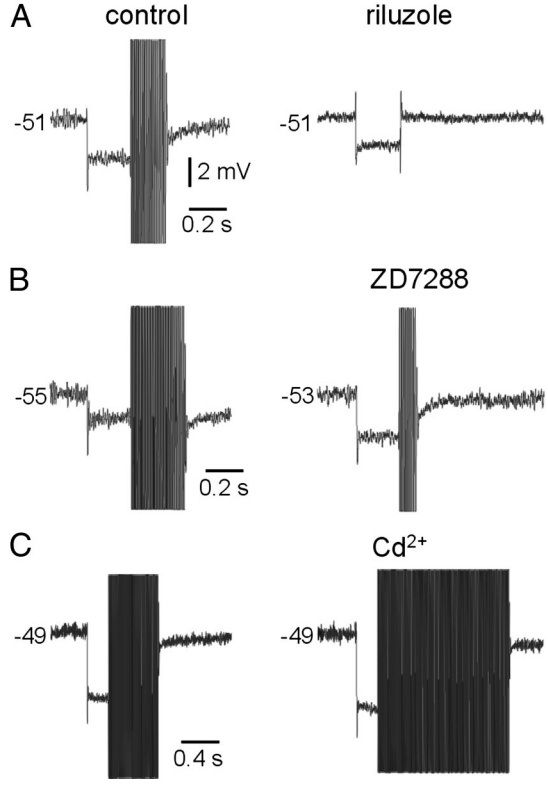

FIG. 7. *A*: postinhibitory response (PIR) was suppressed following riluzole (5 μM). *B*: I_h blocker ZD7288 (10 μM) reduced the duration of PIR, but did not abolished PIR. *C*: PIR duration was enhanced in the presence of Cd^{2+} (100 μM).

Model simulations replicate experimental data

Computer simulations using a Hodgkin-Huxley formalism of actual conductance data from Mes V neurons were able to qualitatively reproduce the essential characteristics of Mes V membrane excitability, resonance, subthreshold oscillations, PIR, and burst generation, as well as to permit us to make predictions as to the role of particular ion channels in production of these membrane behaviors. Since a 4-AP–sensitive K^+ current ($I_{4\text{-AP}}$) is responsible for the large amplitude postspike after hyperpolarization and membrane resonance in these neurons, and gK/Ca is not required for bursting (Wu et al. 2001), we included only this voltage-dependent K^+ conductance, as well as a leakage K^+ conductance, in the model (Del Negro and Chandler 1997).

Model simulations reproduce resonance and subthreshold oscillation behavior

Qualitatively, the response of the model neuron was similar to that of real Mes V neurons. At hyperpolarized membrane potentials, the FRC exhibited a monotonic decrease as a function of ZAP frequency, resembling a low-pass filter. At more depolarized holding potentials, a hump in the FRC emerged and was maximal around –58 mV (Fig. 8*A*). Furthermore, the model exhibited the requisite voltage-dependent subthreshold oscillations experimentally observed at the more depolarized holding potentials (Fig. 8*B*), with frequencies in the range previously reported (Wu et al. 2001).

Previously, we hypothesized that the resonant peak in the FRC results from the interaction of a resonant $I_{4\text{-AP}}$ and the passive membrane properties (Wu et al. 2001). Additionally, it was proposed that the resonance is amplified by I_{NaP}. The simulations replicated these experimental phenomena very well, as shown in Fig. 8*C*. When g_{NaP} was reduced by 10%, the resonant peak was substantially reduced, but the frequency where the peak occurred was minimally altered (Fig. 8*C*). Furthermore, the amplitudes of the subthreshold oscillations were reduced (Fig. 8*D*), indicating that I_{NaP} amplifies resonance and is responsible for the emergence of the subthreshold oscillations. In contrast, when we eliminated $g\text{K}_{4\text{-AP}}$ in the presence of low g_{NaP}, the FRC was transformed into one resembling a low-pass filter (Fig. 8*C*), showing that $I_{4\text{-AP}}$ is a resonant current, and supporting our original hypotheses regarding the roles for these currents in production of resonance in Mes V neurons.

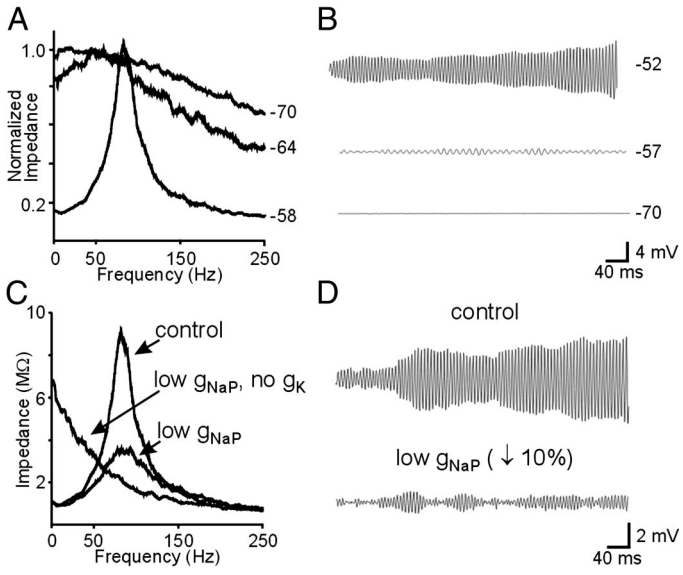

FIG. 8. Model data simulate subthreshold oscillations and resonance. *A*: computer simulation of FRC as a function of holding potential. *B*: simulation of subthreshold oscillations as a function of holding potential. *C*: effects on FRC of altering g_{NaP} and g_{K}. *D*: dependence of subthreshold oscillations on g_{NaP}.

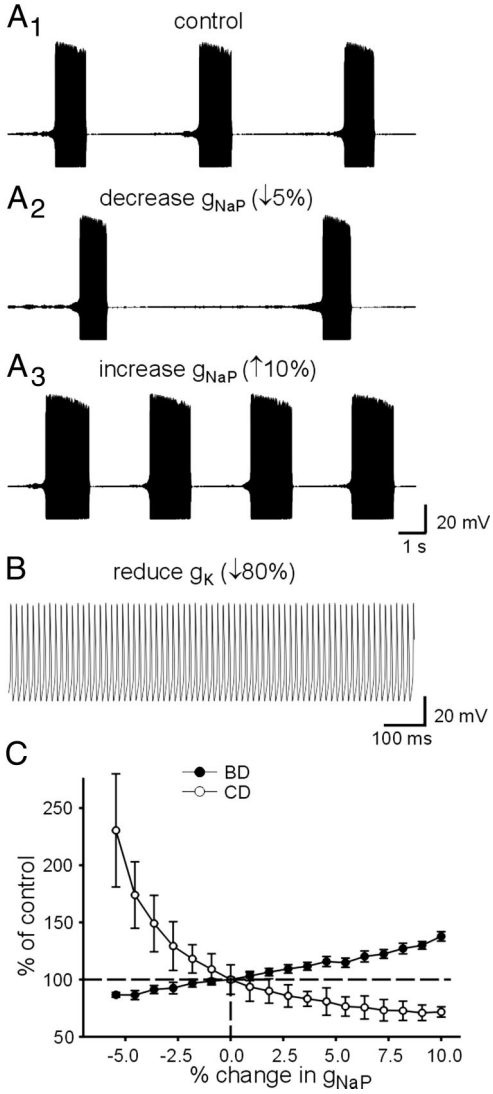

FIG. 9. Bursting is dependent on g_{NaP}. *A1–A3*: effects of altering g_{NaP} on bursting. *B*: reduction of g_{K} transforms bursting into tonic discharge. *C*: effects of altering g_{NaP} on burst duration and cycle duration. Data normalized to 100% (control, dotted line), and each point represents ≥5 consecutive bursts.

Model simulations reproduce bursting characteristics

The model simulation produced bursting characteristics that were very similar to those obtained experimentally. The main effect of lowering g_{NaP} in the model was on CD as opposed to BD. When we lowered the g_{NaP} conductance by as little as 5%, the mean burst CD, based on >10 consecutive model bursts, was prolonged by 70%, whereas the mean BD was decreased modestly (~15%; Fig. 9, *A1*, *A2*, and *C*). In contrast, increasing g_{NaP} shortened CD and prolonged BD (Fig. 9*A3*). As

shown in Fig. 9*C*, a small reduction in g_{NaP} produced significantly far greater changes in CD compared with BD. Interestingly, in the model, the threshold for complete suppression of bursting occurred when g_{NaP} was reduced by around 6%. These data resemble the experimental effects of riluzole on cycle characteristics before complete suppression of bursting (see Fig. 5*C*). Although we don't know the effective concentration of riluzole in the tissue, the main effect of drug application was on cycle duration as opposed to burst duration. Finally, when $I_{4\text{-}AP}$ was reduced by 80% in the model (Fig. 9*B*), the burst discharge was transformed into tonic spike activity. During these conditions, the steep AHP following an evoked action potential was reduced from a peak occurring at –76 to –62 mV, qualitatively similar to that observed experimentally when low doses of 4-AP are applied (Wu et al. 2001).

Previously, we showed that the amplitude of the subthreshold oscillations were largest just before burst generation and were smallest at burst termination (Wu et al. 2001). This phenomenon was replicated by the model simulation (Fig. 10*A*). We suggested that this could result from slow I_{NaP} inactivation during the burst, which would lead to a net loss of inward current. This would then result in burst termination and suppression of subthreshold oscillations following the burst. Recovery from slow I_{NaP} inactivation during the interburst period would then amplify the oscillations and initiate a subsequent burst. Figure 10*A2* shows that, indeed, reduction of g_{NaP} by 10% reduces the amplitude of the oscillations to a level comparable with that observed immediately after burst termination (Fig. 10*A1*), further supporting our hypothesis that I_{NaP} inactivation during the burst would contribute to burst termination via reduction in the underlying mechanisms responsible for subthreshold oscillation amplitude.

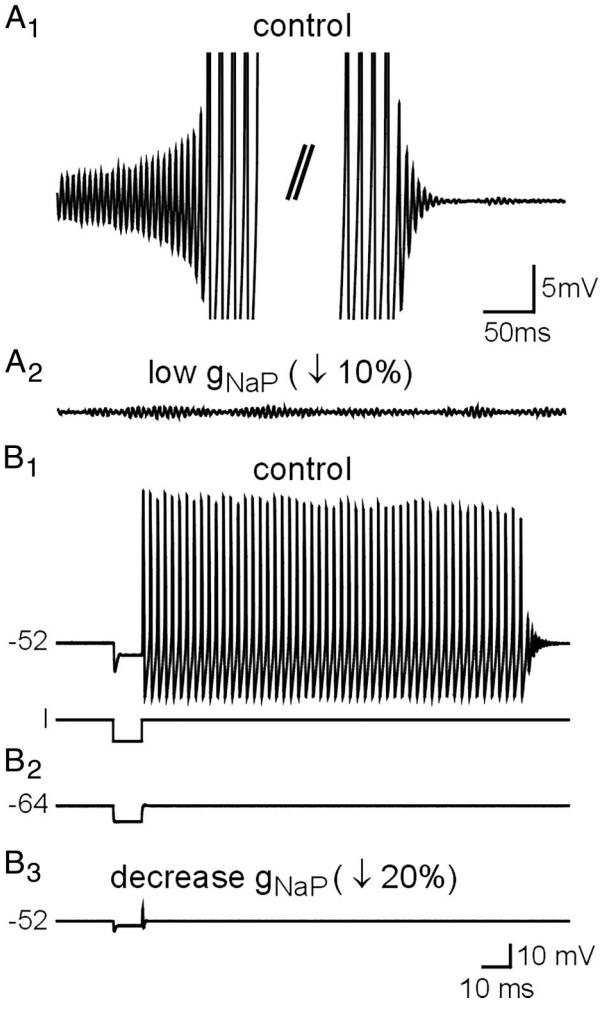

FIG. 10. Burst termination and PIR depend on I_{NaP}. *A1*: subthreshold oscillations are largest before a burst and smallest at burst termination. Slanted vertical lines indicated time break in burst. *A2*: reduction of g_{NaP} produces oscillations that are similar in size to those at the termination of bursting. *B1–B3*: PIR depends on g_{NaP}.

Properties of I_{NaP} and I_{NaT} can account for postinhibitory excitation

As shown in Fig. 7, Mes V neurons show a robust PIR in response to a small amplitude hyperpolarizing current pulse sufficient to change the membrane potential by as little as 3 mV. The model simulation exhibited this behavior (Fig. 10*B1*, *top trace*). At more negative voltages, this behavior was not observed (Fig. 10*B2*). The importance of I_{NaP} is shown in Fig. 10*B3*. Reduction of g_{NaP} by 20% completely suppressed PIR.

DISCUSSION

This study shows that Mes V neurons possess a slowly inactivating sodium current that significantly contributes to control of subthreshold membrane excitability and spike discharge and is not solely a result of a "window current" of the fast transient sodium channel overlap of activation and inactivation gating variables. Specifically, we showed that this current amplifies membrane resonance and is responsible for the emergence of subthreshold oscillations and conditional burst discharge, as well as contributes to the phenomena of postinhibitory discharge. Importantly, we characterized in detail the properties of both the fast transient and slowly inactivating sodium currents, and in conjunction with our previous biophysical data on K^+ currents (Del Negro and Chandler 1997), constructed a neuronal model based on experimental data that replicates many of the salient features of Mes V subthreshold and suprathreshold behavior, thus supporting our original hypothesis as to the ionic origin of these phenomena. The model now affords us the opportunity to generate and test experimentally additional hypotheses regarding the effects of neuromodulators on these currents and subsequent neuronal excitability and burst discharge.

Properties of persistent sodium current

Based on slow ramp voltage commands, all Mes V neurons exhibited I_{NaP} that varied considerably in amplitude between neurons and is consistent with that reported in our previous study (Wu et al. 2001). This current activated at –76 mV, which is ~20 mV more negative to the I_{NaT} measured in these neurons, and exhibited a $V_{1/2max}$ around −60 mV with full activation occurring at approximately −40 mV. In contrast, the $V_{1/2max}$ for the fast transient sodium current was far more positive ($V_{1/2max}$ = −43 mV) than that observed for I_{NaP}. These data are similar to that reported for dissociated dorsal root ganglion neurons (Baker and Bostock 1997), striatal neurons (Cepeda et al. 1995), and entorhinal cortical neurons (Magistretti and Alonso 1999) among others, and suggest that

the persistent current will influence membrane excitability in the subthreshold region.

A significant observation was that, in all Mes V neurons examined, reducing the rate of the ramp voltage command reduced the amplitude of the peak I_{NaP}, suggesting that this current slowly inactivates over the time period examined, similar to that shown in cortical and suprachiasmatic neurons (Fleidervish and Gutnick 1996; Magistretti and Alonso 1999; Pennartz et al. 1997). In our study, the inactivation was never complete and had a component that persisted and represented about 25% of the maximal g_{NaP}, similar to that reported by others (Do and Bean 2003; Fleidervish and Gutnick 1996). Using long conditioning prepulses, we found that inactivation started around −100 mV, with a $V_{1/2max}$ around −58 mV. When examined with conditioning prepulses of various durations, we found that the time constant for onset of inactivation and recovery from inactivation were both around 2 s, within a range similar to that previously reported (Magistretti and Alonso 1999). Furthermore, when using a conditioning action potential command waveform to more closely mimic physiological conditions during bursting (Fig. 6), I_{NaP} was reduced at the end compared with the onset of the burst template, indicating some participation of slow inactivation. Can this small change lead to burst termination? Our model data indicate that as little as a 6% reduction in g_{NaP} will produce cessation of bursting. Therefore it is conceivable that a slight reduction in I_{NaP} could tip the balance between Na^+ and K^+ currents necessary to maintain a burst and result in burst termination. In support of this, the amplitude of the subthreshold oscillations immediately following a burst compared with burst onset are substantially reduced (Wu et al. 2001), and this behavior is replicated in the model (Fig. 10*A*). Additional mechanisms, such as slow inactivation of the I_{NaT} and/or resurgent sodium currents (Do and Bean 2003; Fleidervish and Gutnick 1996) undoubtedly contribute to burst termination as well. Finally, these neurons are endowed with a variety of ionic channels, such as calcium-activated K^+ channels (Del Negro and Chandler 1997; Wu et al. 2001), that likely contribute also to burst termination as well.

Mechanism for the persistent sodium current

Presently, the mechanism(s) responsible for production of the persistent, slowly inactivating sodium current in any neuron type is not clear. This study showed that the slowly inactivating sodium current observed in Mes V neurons cannot be attributed exclusively to a "window current" of the I_{NaT} (for alternative view, see Taddese and Bean 2002). This conclusion is based on comparison of the properties of the measured I_{NaP} with the calculated "window current" of the I_{NaT} measured in the same neurons, and is similar to that concluded for other neuron types (Kay et al. 1998; Magistretti and Alonso 1999; Parri and Crunelli 1998). Although not definitive, the observation that riluzole differentially affected I_{NaP} and I_{NaT} further supports the view that an additional mechanism is involved. Although the molecular mechanisms for different gating modes are not well understood (Alzheimer et al. 1993), the CNS does express a number of different alpha subunits for sodium channels (Goldin 1999). It is unlikely that a single type of sodium channel isoform is responsible for I_{NaP}. Rather, it is more likely that some sodium channel isoforms have a bias for exhibiting one gating mode over another (Alzheimer et al. 1993; Maurice et al. 2001; Patton et al. 1994; Raman and Bean 1997; Smith and Goldin 1998).

Persistent sodium current and control of membrane excitability

In a variety of neurons, persistent calcium or sodium inward currents have been given roles as amplifiers of membrane current and subsequent voltages (Lee and Heckman 1998; Powers and Binder 2003) due to the apparent increase in membrane resistance that occurs before spike threshold (Agrawal et al. 2001; Chandler et al. 1994; Gutfreund et al. 1995; Hsiao et al. 1998; Schwindt and Crill 1995). For instance, in trigeminal motoneurons, I_{NaP} and L-type calcium currents participate in initiation of 5-HT induced burst generation (Hsaio et al. 1998) and amplifying subthreshold membrane potential responses to current pulses (Chandler et al. 1994). In thalamic neurons, persistent currents enhance calcium T-type currents and contribute to low threshold bursting (Parri and Crunelli 1998). In addition to their effects on intrinsic membrane currents, amplification of subthreshold excitatory postsynaptic potentials (EPSPs) by dendritic I_{NaP} or L-type calcium channel activation have also been reported (Lee and Heckman 2000; Lipowsky et al. 1996; Schwindt and Crill 1995).

Persistent sodium currents are implicated in the genesis of subthreshold membrane oscillations in various kinds of neurons (Agrawal et al. 2001; Boehmer et al. 2000; Gutfreund et al. 1995; Reboreda et al. 2003), including mesencephalic trigeminal neurons (Wu et al. 2001). Previously, we showed that Mes V neurons exhibit high-frequency (50–100 Hz) membrane resonance due to the dynamic interaction between the passive resistive-capacitive network and a nonor slowly inactivating 4-AP–sensitive K^+ current. We proposed that activation of I_{NaP} amplifies the resonance and is the basis for subthreshold oscillations (Wu et al. 2001). Although not completely selective, we found that ≤5 μM of riluzole suppressed predominately the I_{NaP} by >80% with usually less than an 11% change in I_{NaT} similar to another study (Urbani and Belluzzi 2000). Additionally, riluzole had no effect on the availability curve for I_{NaT} (Fig. 4*A3*). In the presence of riluzole, the resonant peak amplitude of the FRC (Fig. 4*C*) and the amplitude of the subthreshold oscillations (Fig. 5*B*) were potently suppressed without significant effects on the frequency of the oscillations. During these conditions, the amplitude and threshold of the action potential were minimally affected (Fig. 5D; Table 1). This was not due to suppression of calcium conductances (Huang et al. 1997) since Cd^{2+} produces minimal effects on resonance and subthreshold oscillations (Wu et al. 2001).

Using a minimal neuronal model that included voltage-dependent I_{NaP}, I_{NaT}, and $I_{K4\text{-}AP}$, as well as a leakage K^+ conductance, we found that the model FRC relationship produced a voltage-dependent resonant peak within the frequency ranges reported experimentally (Wu et al. 2001) and was potently suppressed when the I_{NaP} conductance was reduced (Fig. 8), similar to what was experimentally produced by riluzole application (Fig. 5). Furthermore, the model showed that at hyperpolarized holding potentials or after 4-AP application, the resonant peak was abolished and transformed into a

relationship that resembled a typical low-pass filter, as shown experimentally (Wu et al. 2001). Additionally, the model simulated the voltage-dependent emergence of subthreshold oscillations. These data strongly suggest that the I_{NaP} amplifies the membrane resonance and is the basis for the emergence of the subthreshold oscillations, as previously shown in cortical neurons (Gutfreund et al. 1995; reviewed in Hutcheon and Yarom 2000). Persistent sodium currents were also shown to mediate subthreshold oscillations in dorsal column nuclei neurons (Reboreda et al. 2003), and entorhinal cortical neurons, but in the latter, a link to membrane resonance was not shown (Agrawal et al. 2001). Additionally, subthreshold oscillations have been associated with onset of ectopic discharge in DRG neurons after spinal nerve ligation (Liu et al. 2000), and membrane resonance was proposed as the basis for the subthreshold oscillations (Amir et al. 2002). However, a role for I_{NaP} was not studied.

A significant finding in this study was that riluzole completely suppressed burst generation and PIR in Mes V cells in the absence of cessation of spike generation (Fig. 5). Similarly, in respiratory pacemaker neurons, riluzole at the dose sufficient to abolish bursting produced minimal changes in the action potential amplitude (Del Negro et al. 2002). The reduction of bursting in Mes V neurons most likely resulted from suppression of the subthreshold oscillations due to reduction of I_{NaP}, and this was simulated by the model in response to a reduction of g_{NaP} (Fig. 9). In support of this, the model indicated that the amplitudes of the subthreshold oscillations were reduced at burst termination (Fig. 10) and recovered with a time course consistent with the experimentally determined time constant for recovery from I_{NaP} inactivation (Fig. 2) and onset of bursting. Finally, the model predicted that the predominate effect of reduction of g_{NaP} is to significantly prolong cycle duration before complete burst cessation, while producing minimal reduction of burst duration (Fig. 9). This was confirmed experimentally (Fig. 5*C*).

The relatively depolarized $h\infty$ $V_{1/2max}$ for both the persistent sodium and fast transient sodium conductance, compared with that seen in other neuron types, predicted a robust PIR in Mes V neurons, as shown in a previous neuronal modeling study of dorsal root ganglia neurons (Herzog et al. 2001). Although it is not possible to selectively remove the transient sodium conductance experimentally without abolishing action potential initiation in Mes V neurons, reduction of the persistent Na^+ conductance experimentally with riluzole, or in the model, potently reduced PIR, suggesting a role for I_{NaP}. Although the mechanism for this was not examined in detail, the reduction was not due to effects on the fast action potential (Song et al. 1997) or on calcium conductances (Huang et al. 1997), since riluzole was without effect on the transient sodium $h\infty$ $V_{1/2max}$ (Fig. 4), produced small changes in the action potential characteristics (Table 1), and block of calcium channels with Cd^{2+} actually increased PIR (Fig. 7*C*).

Physiological significance

The control of spike generation and bursting is critical to the functioning of any neuronal network, and it has become increasingly apparent that persistent voltage-dependent inward currents such as those using sodium or calcium and active in the subthreshold region contribute significantly to these functions (Do and Bean 2003; Lee and Heckman 2001; Parri and Crunelli 1998; Pennartz et al. 1997; Su et al. 2001; Washburn et al. 2000; see Del Negro et al. 2002 for alternative view). Mes V neurons are unique in that their cell bodies are located within the brain stem and can potentially function as interneurons (Kolta et al. 1995). It is tempting to speculate that the amplified resonance and subthreshold oscillations leading to bursting provide Mes V neurons the ability to participate in oral-motor pattern generation. In fact, synaptic stimulation of areas adjacent to the trigeminal motor nucleus enhances subthreshold oscillations and initiates spiking in Mes V neurons (Verdier et al. 2004). Since Mes V neurons are electrically coupled (Baker and Llinas 1971), this enhancement could serve as a mechanism for synchronizing activity within the Mes V nucleus (Verdier et al. 2004; Wu et al. 2001). Unfortunately, until these circuits are clearly delineated a role for subthreshold oscillations and resonance in pattern generation cannot be established. However, in DRG neurons, it was shown recently that enhanced ectopic discharge resulting from spinal nerve injury is associated with chronic pain and an increased prevalence of subthreshold oscillations (Amir et al. 1999, 2002; Liu et al. 2000). It will be interesting to determine if abnormal jaw movements as a result of injury or disease are related to ectopic discharge in Mes V neurons and result from enhanced membrane resonance and subthreshold oscillations as well. Clearly, any neuromessenger that can alter the resonant properties of the target neuron and the characteristics of subthreshold oscillations will affect Mes V membrane excitability and the effectiveness of cellular communication to these neurons. Studies on modulation of Mes V resonant properties and I_{NaP} should be informative.

ACKNOWLEDGMENTS

We thank M. Castillo for technical assistance.

GRANTS

This work was supported by National Institute of Dental and Craniofacial Research Grant DE-06193.

REFERENCES

Agrawal N, Hamam BN, Magistretti J, Alonso A, and Ragsdale DS. Persistent sodium channel activity mediates subthreshold membrane potential oscillations and low-threshold spikes in rat entorhinal cortex layer V neurons. *Neuroscience* 102: 53–64, 2001.

Alzheimer C. A novel voltage-dependent cation current in rat neocortical neurones. *J Physiol* 479: 199–205, 1994.

Alzheimer C, Schwindt PC, and Crill WE. Modal gating of Na^+ channels as a mechanism of persistent Na^+ current in pyramidal neurons from rat and cat sensorimotor cortex. *J Neurosci* 13: 660–673, 1993.

Amir R, Michaelis M, and Devor M. Membrane potential oscillations in dorsal root ganglion neurons: role in normal electrogenesis and neuropathic pain. *J Neurosci* 19: 8589–8596, 1999.

Amir R, Michaelis M, and Devor M. Burst discharge in primary sensory neurons: triggered by subthreshold oscillations, maintained by depolarizing afterpotentials. *J Neurosci* 22: 1187–1198, 2002.

Baker MD and Bostock H. Low-threshold, persistent sodium current in rat large dorsal root ganglion neurons in culture. *J Neurophysiol* 77: 1503–1513, 1997.

Baker R and Llinas R. Electrotonic coupling between neurones in the rat mesencephalic nucleus. *J Physiol* 212: 45–63, 1971.

Boehmer G, Greffrath W, Martin E, and Hermann S. Subthreshold oscillation of the membrane potential in magnocellular neurones of the rat supraoptic nucleus. *J Physiol* 526: 115–128, 2000.

Butera RJ Jr, Rinzel J, and Smith JC. Models of respiratory rhythm generation in the pre-Botzinger complex. I. Bursting pacemaker neurons. *J Neurophysiol* 82: 382–397, 1999.

Cepeda C, Chandler SH, Shumate LW, and Levine MS. Persistent Na^+ conductance in medium-sized neostriatal neurons: characterization using infrared videomicroscopy and whole cell patch-clamp recordings. *J Neurophysiol* 74: 1343–1348, 1995.

Chandler SH, Hsaio CF, Inoue T, and Goldberg LJ. Electrophysiological properties of guinea pig trigeminal motoneurons recorded in vitro. *J Neurophysiol* 71: 129–145, 1994.

Crill WE. Persistent sodium current in mammalian central neurons. *Annu Rev Physiol* 58: 349–362, 1996.

Dale N. Kinetic characterization of the voltage-gated currents possessed by *Xenopus* embryo spinal neurons. *J Physiol* 489:473–488, 1995.

Del Negro CA, and Chandler SH. Physiological and theoretical analysis of K^+ currents controlling discharge in neonatal rat mesencephalic trigeminal neurons. *J Neurophysiol* 77: 537–553, 1997.

Del Negro CA, Morgado-Valle C, and Feldman JL. Respiratory rhythm: an emergent network property? *Neuron* 34: 821–830, 2002.

Do MT and Bean BP. Subthreshold sodium currents and pacemaking of subthalamic neurons: modulation by slow inactivation. *Neuron* 39: 109–120, 2003.

Fleidervish IA and Gutnick MJ. Kinetics of slow inactivation of persistent sodium current in layer V neurons of mouse neocortical slices. *J Neurophysiol* 76: 2125–2130, 1996.

Goldin AL. Diversity of mammalian voltage-gated sodium channels. *Ann N Y Acad Sci* 868: 38–50, 1999.

Goldin AL. Resurgence of sodium channel research. *Annu Rev Physiol* 63: 871–894, 2001.

Gutfreund Y, Yarom Y, and Segev I. Subthreshold oscillations and resonant frequency in guinea-pig cortical neurons: physiology and modelling. *J Physiol* 483: 621–640, 1995.

Henderson G, Pepper CM, and Shefner SA. Electrophysiological properties of neurons contained in the locus coeruleus and mesencephalic nucleus of the trigeminal nerve in vitro. *Exp Brain Res* 45: 29–37, 1982.

Herzog RI, Cummins TR, and Waxman SG. Persistent TTX-resistant Na^+ current affects resting potential and response to depolarization in simulated spinal sensory neurons. *J Neurophysiol* 86: 1351–1364, 2001.

Hsiao CF, Del Negro CA, Trueblood PR, and Chandler SH. Ionic basis for serotonin-induced bistable membrane properties in guinea pig trigeminal motoneurons. *J Neurophysiol* 79: 2847–2856, 1998.

Hu H, Vervaeke K, and Storm JF. Two forms of electrical resonance at theta frequencies, generated by M-current, h-current and persistent Na^+ current in rat hippocampal pyramidal cells. *J Physiol* 545: 783–805, 2002.

Huang CS, Song JH, Nagata K, Yeh JZ, and Narahashi T. Effects of the neuroprotective agent riluzole on the high voltage-activated calcium channels of rat dorsal root ganglion neurons. *J Pharmacol Exp Ther* 282: 1280–1290, 1997.

Hutcheon B and Yarom Y. Resonance, oscillation and the intrinsic frequency preferences of neurons. *Trends Neurosci* 23: 216–222, 2000.

Kay AR, Sugimori M, and Llinas R. Kinetic and stochastic properties of a persistent sodium current in mature guinea pig cerebellar Purkinje cells. *J Neurophysiol* 80: 1167–1179, 1998.

Klink R and Alonso A. Ionic mechanisms for the subthreshold oscillations and differential electroresponsiveness of medial entorhinal cortex layer II neurons. *J Neurophysiol* 70: 144–157, 1993.

Kolta A, Lund JP, Westberg KG, and Clavelou P. Do muscle-spindle afferents act as interneurons during mastication? *Trends Neurosci* 18:441, 1995.

Lee RH and Heckman CJ. Bistability in spinal motoneurons in vivo: systematic variations in persistent inward currents. *J Neurophysiol* 80: 583–593, 1998.

Lee RH and Heckman CJ. Adjustable amplification of synaptic input in the dendrites of spinal motoneurons in vivo. *J Neurosci* 20: 6734–6740, 2000.

Lee RH and Heckman CJ. Essential role of a fast persistent inward current in action potential initiation and control of rhythmic firing. *J Neurophysiol* 85: 472–475, 2001.

Lipowsky R, Gillessen T, and Alzheimer C. Dendritic Na^+ channels amplify EPSPs in hippocampal CA1 pyramidal cells. *J Neurophysiol* 76: 2181–2191, 1996.

Liu CN, Michaelis M, Amir R, and Devor M. Spinal nerve injury enhances subthreshold membrane potential oscillations in DRG neurons: relation to neuropathic pain. *J Neurophysiol* 84: 205–215, 2000.

Llinas R and Yarom Y. Properties and distribution of ionic conductances generating electroresponsiveness of mammalian inferior olivary neurones in vitro. *J Physiol* 315: 569–584, 1981.

Magistretti J and Alonso A. Biophysical properties and slow voltage-dependent inactivation of a sustained sodium current in entorhinal cortex layer-II principal neurons: a whole-cell and single-channel study. *J Gen Physiol* 114: 491–509, 1999.

Maurice N, Tkatch T, Meisler M, Sprunger LK, and Surmeier DJ. D1/D5 dopamine receptor activation differentially modulates rapidly inactivating and persistent sodium currents in prefrontal cortex pyramidal neurons. *J Neurosci* 21: 2268–2277, 2001.

McCormick DA, and Pape HC. Properties of a hyperpolarization-activated cation current and its role in rhythmic oscillation in thalamic relay neurones. *J Physiol* 431: 291–318, 1990.

Parri HR and Crunelli V. Sodium current in rat and cat thalamocortical neurons: role of a non- inactivating component in tonic and burst firing. *J Neurosci* 18: 854–867, 1998.

Patton DE, Isom LL, Catterall WA, and Goldin AL. The adult rat brain beta 1 subunit modifies activation and inactivation gating of multiple sodium channel alpha subunits. *J Biol Chem* 269: 17649–17655, 1994.

Pennartz CM, Bierlaagh MA, and Geurtsen AM. Cellular mechanisms underlying spontaneous firing in rat suprachiasmatic nucleus: involvement of a slowly inactivating component of sodium current. *J Neurophysiol* 78: 1811–1825, 1997.

Powers RK and Binder MD. Persistent sodium and calcium currents in rat hypoglossal motoneurons. *J Neurophysiol* 89: 615–624, 2003.

Puil E, Gimbarzevsky B, and Miura RM. Quantification of membrane properties of trigeminal root ganglion neurons in guinea pigs. *J Neurophysiol* 55: 995–1016, 1986.

Puil E, Gimbarzevsky B, and Spigelman I. Primary involvement of K^+ conductance in membrane resonance of trigeminal root ganglion neurons. *J Neurophysiol* 59: 77–89, 1988.

Raman IM and Bean BP. Resurgent sodium current and action potential formation in dissociated cerebellar Purkinje neurons. *J Neurosci* 17: 4517–4526, 1997.

Reboreda A, Sanchez E, Romero M, and Lamas JA. Intrinsic spontaneous activity and subthreshold oscillations in neurones of the rat dorsal column nuclei in culture. *J Physiol* 551: 191–205, 2003.

Schurr A, West CA, and Rigor BM. Lactate-supported synaptic function in the rat hippocampal slice preparation. *Science* 240: 1326–1328, 1988.

Schwindt PC and Crill WE. Amplification of synaptic current by persistent sodium conductance in apical dendrite of neocortical neurons. *J Neurophysiol* 74: 2220–2224, 1995.

Smith RD and Goldin AL. Functional analysis of the rat I sodium channel in xenopus oocytes. *J Neurosci* 18: 811–820, 1998.

Song JH, Huang CS, Nagata K, Yeh JZ, and Narahashi T. Differential action of riluzole on tetrodotoxin-sensitive and tetrodotoxin-resistant sodium channels. *J Pharmacol Exp Ther* 282: 707–714, 1997.

Stuart GJ, Dodt HU, and Sakmann B. Patch-clamp recordings from the soma and dendrites of neurons in brain slices using infrared video microscopy. *Pfluegers* 423: 511–518, 1993.

Su H, Alroy G, Kirson ED, and Yaari Y. Extracellular calcium modulates persistent sodium current-dependent burst-firing in hippocampal pyramidal neurons. *J Neurosci* 21: 4173–4182, 2001.

Taddese A and Bean BP. Subthreshold sodium current from rapidly inactivating sodium channels drives spontaneous firing of tuberomammillary neurons. *Neuron* 33: 587–600, 2002.

Tanaka S, Wu N, Hsaio CF, Turman J Jr, and Chandler SH. Development of inward rectification and control of membrane excitability in mesencephalic v neurons. *J Neurophysiol* 89: 1288–1298, 2003.

Urbani A and Belluzzi O. Riluzole inhibits the persistent sodium current in mammalian CNS neurons. *Eur J Neurosci* 12: 3567–3574, 2000.

Verdier D, Lund JP, and Kolta A. Synaptic inputs to trigeminal primary afferent neurons cause firing and modulate intrinsic oscillatory activity. *J Neurophysiol* 92: 2444–2455, 2004.

Washburn DL, Anderson JW, and Ferguson AV. A subthreshold persistent sodium current mediates bursting in rat subfornical organ neurones. *J Physiol* 529: 359–371, 2000.

Waxman SG. Chair's introduction: sodium channels and neuronal dysfunction–emerging concepts, converging themes. *Novartis Found Symp* 241: 1–4, 2002.

Wu N, Hsiao CF, and Chandler SH. Membrane resonance and subthreshold membrane oscillations in mesencephalic V neurons: participants in burst generation. *J Neurosci* 21: 3729–3739, 2001.

Zhang L and Krnjevic K. Whole-cell recording of anoxic effects on hippocampal neurons in slices. *J Neurophysiol* 69: 118–127, 1993.